J Neuropathol Exp Neurol
Vol. 75, No. 2, February 2016, pp. 183–196
doi: 10.1093/jnen/nlv019

ORIGINAL ARTICLE

A Compact Blast-Induced Traumatic Brain Injury Model in Mice

Hongxing Wang, MD, Yi Ping Zhang, MD, Jun Cai, MD, PhD, Lisa B. E. Shields, MD, Chad A. Tuchek, BS, Riyi Shi, MD, PhD, Jianan Li, PhD, Christopher B. Shields, MD, and Xiao-Ming Xu, MD, PhD

Abstract

Blast-induced traumatic brain injury (bTBI) is a common injury on the battlefield and often results in permanent cognitive and neurological abnormalities. We report a novel compact device that creates graded bTBI in mice. The injury severity can be controlled by precise pressures that mimic Friedlander shockwave curves. The mouse head was stabilized with a head fixator, and the body was protected with a metal shield; shockwave durations were 3 to 4 milliseconds. Reflective shockwave peak readings at the position of the mouse head were 12 ± 2.6 psi, 50 ± 20.3 psi, and 100 ± 33.1 psi at 100, 200, and 250 psi predetermined driver chamber pressures, respectively. The bTBIs of 250 psi caused 80% mortality, which decreased to 27% with the metal shield. Brain and lung damage depended on the shockwave duration and amplitude. Cognitive deficits were assessed using the Morris water maze, Y-maze, and open-field tests. Pathological changes in the brain included disruption of the blood-brain barrier, multifocal neuronal and axonal degeneration, and reactive gliosis assessed by Evans Blue dye extravasation, silver and Fluoro-Jade B staining, and glial fibrillary acidic protein immunohistochemistry, respectively. Behavioral and pathological changes were injury severity-dependent. This mouse bTBI model may be useful for investigating injury mechanisms and therapeutic strategies associated with bTBI.

From Spinal Cord and Brain Injury Research Group, Stark Neurosciences Research Institute, Department of Neurological Surgery, Indiana University School of Medicine (HW, CAT, XMX), Indianapolis, Indiana; First Affiliated Hospital of Nanjing Medical University (HW, JL), Nanjing, Jiangsu Province, P. R. China; Norton Neuroscience Institute (YPZ, LBES, CBS), Norton Healthcare, Louisville, Kentucky; Department of Pediatrics, University of Louisville (JC), Louisville, Kentucky; Department of Basic Medical Sciences, Weldon School of Biomedical Engineering, Center for Paralysis Research, Purdue University (RS), West Lafayette, Indiana; Department of Anatomical Sciences and Neurobiology, University of Louisville (CBS), Louisville, Kentucky.

Send correspondence to: Xiao-Ming Xu, MD, PhD, Spinal Cord and Brain Injury Research Group, Stark Neurosciences Research Institute, Indiana University School of Medicine, 320 West 15th Street, NB E500, Indianapolis, IN 46202-2266; E-mail: xu26@iupui.edu

This work was supported in part by the National Key Clinical Specialist Construction Programs and Jiangsu Health International Exchange Program Sponsorship of China (HW), National Institutes of Health (NIH) 1R01 NS059622, R01 NS050243, 1R01 NS073636, the Indiana Spinal Cord and Brain Injury Research Foundation (ISCBIRF), and Mari Hulman George Endowment Funds (XMX).

Key Words: Behavioral assessments, Blast injury, Edema, Neuronal degeneration, Traumatic brain injury.

INTRODUCTION

Blast-induced traumatic brain injury (bTBI) causes significant morbidity to military personnel. bTBIs can be caused by shockwaves emanating from explosions, direct injury from projectiles, acceleration/deceleration injuries, and systemic factors such as hemorrhage, burns, or respiratory arrest. Detailed pathophysiologic mechanisms of brain damage caused by transfer of energy via shockwaves are still unresolved. Understanding neuropathological events and molecular pathways of the bTBI should facilitate the development of effective therapies for patients with bTBI and improve the quality of their lives (1–8).

To develop effective therapeutic strategies for bTBI, reliable and proper experimental models are essential (9). Currently, most experimental bTBI devices consist of a cylinder that is closed at one end and open at the other. The cylinder is divided into 2 compartments. The first compartment is a closed compartment (driver chamber) within which the air pressure can be increased. The shockwave is detonated by the sudden release of compressed air from this compartment. The second compartment is an open ended compartment (driven chamber) within which animals are placed (5, 6, 10–15). A bTBI device must generate a Friedlander wave to which the animal is exposed. The Friedlander wave is characterized by a positive peak that decays exponentially to ambient pressure followed by a negative phase (16). The Friedlander shockwave causes brain damage by creating a shock-bubble effect due to an acoustic impedance mismatch (17). Brain damage may also be produced by increased cerebrovascular volume caused by an increase in intrathoracic pressure (18).

In recent years, genetically modified mice have been widely used to elucidate mechanisms of brain injuries and identify putative therapeutic targets. Although the size and shape of the mouse brain and its susceptibility to bTBI are very different from those of humans, studies in mice with different genetic backgrounds may advance our knowledge of the pathophysiology and mechanisms of bTBI. Mouse models have been used to study therapeutic strategies such as

attenuation of inflammation (19–27), reduction of cellular stress/apoptosis (28–34), and enhancement of recovery (35–39). Mice are cost effective, easy to handle, and can be genetically modified making them a unique species for bTBI research (40–42).

In most experimental bTBI models, the injury severity generated by compressed air is dependent on the structure, strength, and thickness of the membrane placed between the driver and driven chambers (43). In most blast injury systems, the membranes may rupture at different pressures creating bTBI of unpredictable magnitudes. Most blast injury devices are large and vary in length from 6 to 68 feet (6, 10, 14, 44, 45). Here, we report the development of a novel bTBI device that creates graded blast injuries whose intensity can be controlled by precise pressures. Additionally, the size of the device is compact (blast tube length: 100 cm) and can be easily mounted on a table.

MATERIALS AND METHODS

Animals

The studies were conducted in accordance with Guidelines for the Care and Use of Laboratory Animals (National Research Council, USA) and Guidelines of the Indiana Institutional Animal Care and Use Committee. C57/BL6 mice (8 weeks old and weighing 18–20 g) were purchased from Jackson Laboratory (Bar Harbor, ME). Animals were housed under 12-hour light and 12-hour dark conditions with food and water available ad libitum. They were acclimated for 1 week prior to being subjected to the blast injury. A total of 100 male mice were used in this study. Among them, 67 mice were divided into the following groups: sham-operation (n = 15); 100 psi (n = 15); 200 psi (n = 15); and 250 psi (n = 22). Another 23 mice were used in a pilot study to determine the survival rate of mice subjected to 250 psi bTBI without thoracic and nose protection.

Construction of the Blast Injury Apparatus

The dimensions of the metal blast tube were 100 cm long, 7.1 cm wide, and 3.2 cm high (Fig. 1). A circular driver chamber (30.25 cm^2 in cross-sectional area) was connected to a rectangular driven chamber (22.72 cm^2 area). A metal frame held the plastic membrane in an airtight manner between the 2 chambers using 8 screws. A high pressure was created with compressed air in the driver chamber. The mechanism to produce a predetermined shockwave of a specific intensity was determined by the air pressure differential across the membrane placed between the driver and driven chambers. The air pressure within the driver chamber was generated by a double gauge regulator located on a nitrogen tank (Fig. 1A). When the pressure within the driver chamber reached a predetermined level, the membrane was penetrated by a sharp blade located in the driven chamber (Fig. 1A). The blade was triggered by a pneumatic cylinder (50 psi). Following the rupture of the membrane, the shockwave was released. Air was forced from the driver chamber into the driven chamber at the predetermined pressure. The membrane rupture induced a blast in the driven chamber. The shock tube sat on anti-vibration rubber mounts (Fig. 1B). Shockwave intensities generated by 3 different pressures were calibrated using a pressure-sensor attached to the mouse head fixator (Fig. 1C). The mouse head fixator was made from stainless steel that prevented head movement during the blast. A metal bar was attached to the head fixator to control the position of the mouse in the driven chamber.

In this study, the mouse was placed within the driven chamber with the head 60 cm from the membrane. Two polycarbonate membranes (McMaster-Carr, Elmhurst, IL) with thicknesses of 125 and 250 μm were utilized. The 125-μm-thick membrane was used for the 100 psi predetermined pressure; the 250-μm-thick membrane was used for the pressures $\geq$ 200 psi. The pressure for the membrane penetration system was maintained at 50 psi with a mini-pneumatic regulator (Gison Taichung, Taiwan). The rectangular shape of the driven chamber provided a flat surface for the mouse, stabilized in the head fixator.

Shockwave Measurement

Shockwaves were measured using a pressure transducer (model 105C02, PCB Piezotronics, Depew, NY) placed on the head fixator. Outputs from the sensor that measured shockwave intensities (microvolts) were displayed, recorded, and converted to psi units. The transducer was aligned to face the shockwave that was at the same position as the mouse head. Pressures at other locations in the driven chamber or at different angles to the membrane were not monitored. After membranes were ruptured, the maximum positive and negative pressures (mean ± SD) and durations of the shockwaves were recorded.

Safety Measurements at the Blast Site

Potential injuries to the experimental personnel were assessed before performing these experiments. Two potential safety issues to the experimental personnel in the vicinity of the blast include: 1) injury from projectiles emanating from the device, and 2) hearing damage by noise created by the blast. To avoid projectile injuries, the opening of the driven chamber was placed so that the open end faced a wall during the blast. Any evidence of ejected debris was recorded. Because the blast created a loud noise, sound level was monitored in the proximity to the blast. An Amprobe SM-10 Sound Level Meter (Amprobe, Glottertal, Germany) was placed 100 cm away from and aligned with the shock tube opening. A sound intensity exceeding 90 dB was considered harmful.

Blast Exposure

Animals were anesthetized with Isoflurane (2%) in a commercial anesthesia box (Kent Scientific, Torrington, CT). The mouse was stabilized in a holder that was placed in the anesthesia box. After anesthesia, the mouse with the holder was removed from the box and placed within the driven chamber at 60 cm from the membrane while breathing room air. The estimated time for removal of the mouse from the Isoflurane box, insertion into the shock chamber, and subjection

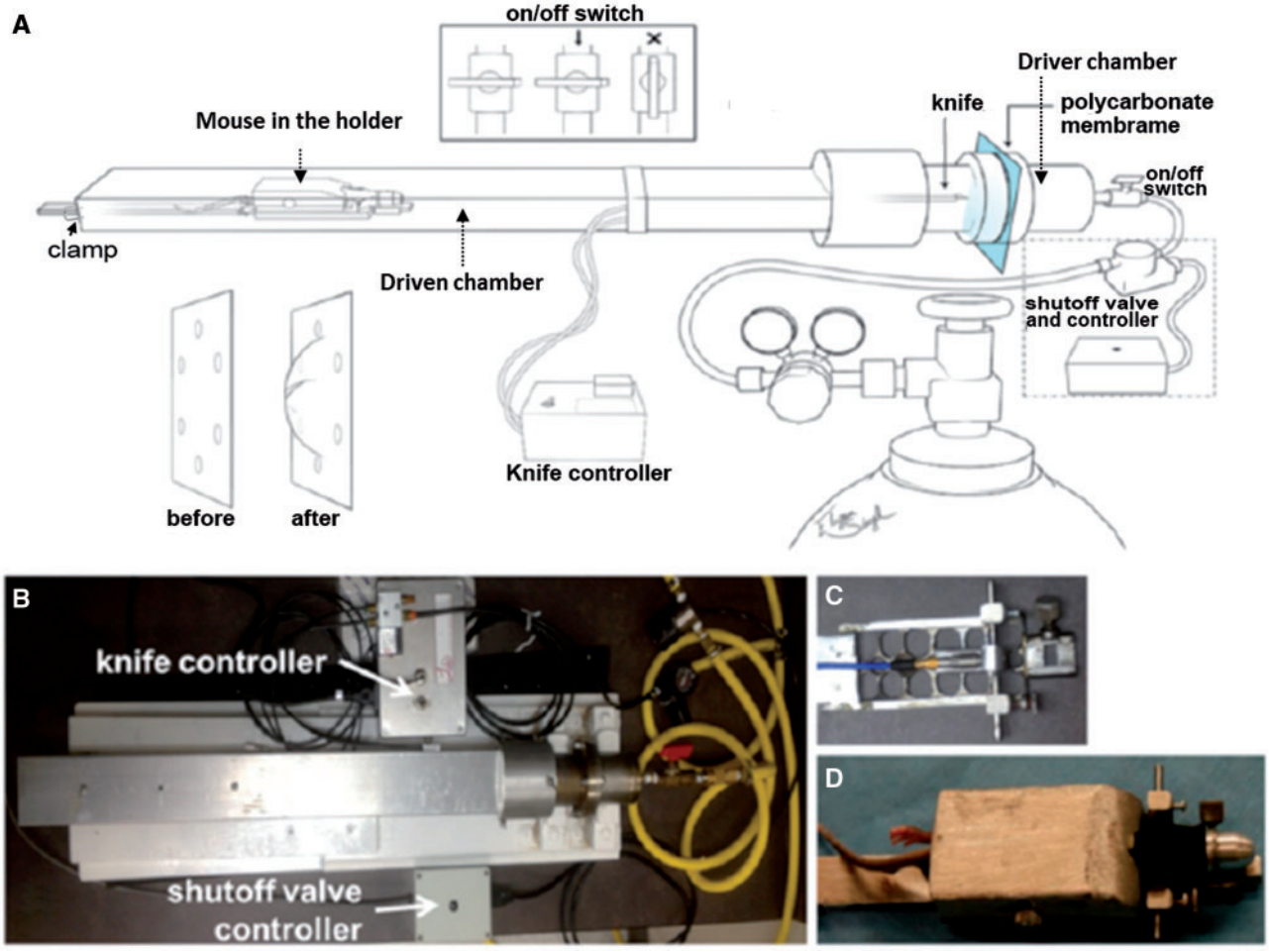

FIGURE 1. The blast injury device: basic components and mechanism of action. **(A)** Schematic drawing illustrates major components of the blast injury device. A polycarbonate membrane (light blue) separates the driver chamber on the right from the driven chamber on the left. The driver chamber can be filled with air to a predetermined pressure. The shutoff valve will be turned off when the pressure reaches a predetermined level. The blast will be created when the membrane is perforated by pressing a switch that activates the knife to move forward within the driven chamber and penetrate the membrane. Within the driven chamber, a mouse was mounted on a head fixator. In the lower left corner, membranes before and after the blast are depicted. **(B)** A top view of the blast injury device with the shock tube seated on an anti-vibration mount. The knife-controlling device is used to trigger membrane perforation; the shutoff valve controls the required air pressure in the driver chamber. **(C)** A pressure sensor served as a phantom attached to the head fixator to measure shockwave forces at the head location. **(D)** A mouse was stabilized on the head fixator, and its body was covered by a metal protective shield to reduce pneumatic barotrauma.

to the blast injury was 30 seconds. This was a shorter time than it took for control mice to regain response to pain after being removed from the anesthesia box (approximately 60 seconds), indicating that mice did not appreciate pain from the blast.

The animal holder was attached to a rod extending from the posterior end of the holder. The rod was securely immobilized in the shock chamber by clamping it to the base of the shock tube. The mouse was centered in the shock chamber tube. Although we did not monitor mouse head motion during the blast, the head was maintained firmly in place by the nose cone and ear bars, and the body was fixed in the holder. The holder and rod were rigidly attached to the base of the shock tube; therefore, if any motion of the head occurred, it would be minimal. This prevented any measurable acceleration/deceleration motion of the head, thereby precluding damage to the brain from that motion.

Chest and Snout Protection on Animal Mortality

A high survival rate of mice exposed to shockwaves is necessary to study bTBI mechanisms. A pilot study indicated that a blast injury of 250 psi caused pulmonary trauma and high mortality. Because body protection may reduce the mortality rate caused by blast-induced lung injury, a nose cone and metal shield covering the body below the neck was designed to protect the lungs from barotrauma (Fig. 1D). The shield dimension was 65 mm long, 30 mm wide and 20 mm high. The height of the shield can be adjusted based on the

ventrodorsal size of the animal's thorax. Properly fitted chest shields did not affect the animal's ability to breathe.

Behavioral Assessment

Behavioral assessment was measured using the Rotarod, Morris water maze, Y-maze, and open field exploration tests. These assays detect changes in neurological, cognitive, and emotional functions, and they were performed as indicated in the timetable (Fig. 2).

The Rotarod test measures sensorimotor function of the animal (46). A 5-lane device (IITC Life Science Inc., Woodland Hills, CA) consists of a metal rod and plastic drum. The width of each lane is 3.18 cm. The Rotarod was accelerated from 1 to 30 rpm over 90 seconds, with each trial lasting for a maximum of 120 seconds. One trial was recorded from the time the Rotarod began turning to the point that the mouse fell off. A baseline Rotarod test was performed on each mouse before being subjected to a bTBI. Five Rotarod tests were performed at 1, 3, and 7 days post-injury, with the average of the middle 3 trials considered to be the Rotarod score.

The Morris water maze test is designed to assess spatial learning and memory (47). The apparatus consists of a circular plastic pool (100 cm in diameter and 60 cm in depth) filled with water to a depth of 30 cm. A clear Plexiglas platform (10 cm in diameter and 29.5 cm in height) was submerged 0.5 cm below the water surface and was located in the midpoint of 1 quadrant, which served as a hidden stage for resting (46). Mice were placed in the pool at 1 of 4 starting positions. In each trial, the time required to reach the platform was recorded. Mice that found the platform were allowed to remain on the platform for 30 seconds and then were returned to their home cage (inter-trial interval). Mice that did not find the platform within 60 seconds were placed on the platform for 30 seconds. Three trials per day were conducted for 5 consecutive days with an inter-trial interval of 5 minutes. On day 6 following the bTBI, the platform was removed from the pool and the trial was performed with a cutoff time of 60 seconds. The duration that the mouse remained in the quadrant that previously contained the platform was recorded as a percentage of the total time in the pool. This test was recorded by video and analyzed by Topscan 3.0 software (Clever Sys Inc., Reston, VA).

The Y-maze is a neurobehavioral test used to measure rodents' innate tendency of exploration and spatial working memory associated with the function of hippocampus, septum, basal forebrain, and prefrontal cortex (48, 49). The Y-maze apparatus consists of 3 opaque plastic corridors at a 120° angle to each other. The corridor is 1.375 inches wide by 7.875 inches long. The test was performed and videotaped in a quiet room illuminated with red light. The mouse was introduced onto the center of the maze and allowed to explore the corridors for 8 minutes. The number and sequence of entries into each corridor was recorded. A complete corridor entry was considered when all 4 limbs were entered. Entry into 3 different corridors in succession (eg, ABC, BCA, CBA, or CAB arms) was considered as 1 alternation. The Y-maze score was calculated by the formula: $= \frac{\text{Total number of alternations}}{(\text{Total number of entries} - 2)} \times 100$.

Mice were tested on days 1 and 7 after the bTBI. The maze was cleaned with 75% ethanol after each test.

The open field exploration test was performed in a quiet, dark room illuminated with red light on day 1 after the bTBI. Each mouse was placed within an 8-inch square central area within a 16-inch square Plexiglas open box with 6-inch-high walls. The mouse was allowed to explore for 10 minutes. During each 10-minute session, the number of times that the mouse entered the central area was recorded. In addition, the percent of time spent in the inner zone compared to the total time spent in the open field was calculated (50, 51). The mouse anxiety level correlated with a decreased duration spent in the central field. The Plexiglas was cleaned with 75% ethanol solution between each trial.

Tissue Preparation

At day 1 post-injury, brains from 20 mice (n = 5/group) were used to measure the integrity of blood-brain barrier

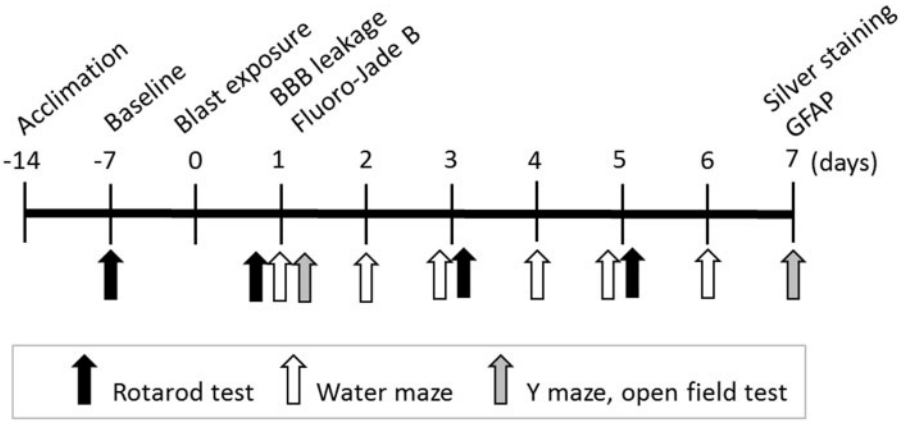

FIGURE 2. Experimental timeline. Mice were acclimated at 14 days before the blast injury, and baseline behavior was assessed at 7 days before injury. The blast exposure was performed at day 0. Blood-brain-barrier (BBB) leakage and Fluoro-Jade B assessments were performed at 1 week after injury. Silver staining and glial fibrillary acidic protein (GFAP) immunostaining were performed at 7 weeks post-injury. The Rotarod test was performed at 1, 3, and 5 days. The Morris water maze was performed every week from week 1 to week 6. The Y maze and open filed test were performed at week 1 and week 7.

(BBB). For Fluoro-Jade B (FJB) staining, mice (n = 5/group) were also flushed with saline followed by 4% paraformaldehyde (PFA) perfusion. For silver staining and glial fibrillary acidic protein (GFAP) immunohistochemistry staining, mice (n = 5/group) were killed at day 7 post-injury by flushing with sodium cacodylate buffer (8 g NaCl, 4 g dextrose, 8 g sucrose, 0.23 g $CaCl_2$, and 0.34 g sodium cacodylate per 1,000 ml H_2O) followed by 4% PFA in cacodylate buffer. The harvested brains were post-fixed in the same fixative overnight.

Brain Tissue Water Content and BBB Assays

The BBB assay measures changes in vascular permeability (52, 53). Twenty-four hours following bTBI, mice (n = 5/group) were anesthetized, and a 33-gauge needle was inserted into the left jugular vein and Evans Blue ([EB] 2%) in saline (4 μl/g of body weight) was slowly injected. Four hours later the dye was washed out of the vascular system with 30 ml of cold saline prior to death. Mice were then killed, and their brains were removed and evaluated for Evans Blue extravasation. The water content of collected brain tissue was measured using the wet/dry weight method (54, 55). The wet weight (WW) of the brain tissue was measured immediately after dissection and then dried at 56°C for 2 days to record the dry weight (DW). The percentage of water content of brain was calculated using the equation: $[(WW - DW/WW)] \times 100$. The dried brain was immersed in formamide (4 ml/g of brain tissue) and incubated at 56°C for 2 days to allow for extraction of EB into a solvent. The EB content was measured with a spectrophotometer at a wavelength of 620 nm. Each sample absorbance value was measured 3 times and converted into the actual value in EB/brain (μg/g) using a standard pre-calibrated concentration curve.

FJB Staining

FJB staining assesses degenerative neuronal and axonal changes in the brain (56, 57). FBJ staining was prepared by incubating brain sections in a 1% alkaline (NaOH) and 80% ethanol solution for 5 minutes, then hydrated in graded ethanol in distilled water (70, 50, 25, and 0%) for 5 minutes each (58). Sections were incubated in 0.06% potassium permanganate for 20 minutes, rinsed in distilled water for 2 minutes, and then incubated in a 0.0004% solution of FJB (EMD Millipore, Billerica, MA) for 20 minutes. Slides were rinsed in distilled water for 2 minutes and dried in air. The dried slides were washed in xylene 2 times for approximately 2 minutes each and mounted with DPX (Sigma-Aldrich, St. Louis, MO).

Silver Staining

After post-fixation in 4% PFA, the brains were dehydrated in 20% sucrose overnight. They were then embedded in 0.5% gelatin solution and cut into 50-μm-thick cryostat sections for silver staining and 25-μm-thick sections for GFAP immunohistochemistry. The silver staining was performed using an amino-cupric silver histochemical technique (59, 60). Briefly, brain sections were incubated in 4% PFA for at least 1 week at 4°C. The sections were immersed into pre-impregnation solution for 1 hour and heated to 50°C for 45 minutes and then cooled to room temperature for 2 to 3 hours. The sections were agitated for 15 to 30 seconds in acetone twice and transferred into diamine-silver solution for 45 to 50 minutes. During incubation the slices were constantly stirred in a diamine-silver covered container on a rotating platform. The slice was placed in a reducer solution (at 32°C) for 25 minutes and gently agitated for 1 to 5 minutes. The diamine solution was added (3 ml/100 ml) 4 times at 5-minute intervals to affect silver impregnation. When dark brown appeared on the slice, they were transferred into distilled water for 1 to 2 minutes. To stop the silver impregnation, the sections were transferred into 0.5% glacial acetic acid solution for 1 to 2 minutes then rinsed 3 times in water (15, 15, and 30 minutes) and stored in dH_2O overnight. On the following day, sections were bleached in acidic ferricyanide solution for 20 to 60 seconds at room temperature until they became semi-transparent. The sections were thoroughly washed in dH_2O and then transferred into a second bleaching solution (consisting of 0.06% potassium permanganate [120 ml] and 5% sulfuric acid [4 ml]) for 15 to 20 seconds until the sections turned pinkish-yellow with an opaque appearance. The sections were washed in water (5 minutes x 2) and then were stabilized in 2% sodium thiosulfate solution with light agitation. After differentiation and stabilization, the sections were rinsed again in water for 2 to 5 minutes, then the color was fixed in a rapid fixer solution (Kodak A+B, 1:6 in dH_2O, Fisher Scientific, Waltham, MA). After the background became transparent, the sections remained in Kodak fixer solution for 5 minutes. Sections were washed in dH_2O, incubated in a 0.5% gelatin and 80% alcohol solution for 5 minutes, and mounted on slides that were air dried. They were then rinsed with distilled water and dehydrated in graded ethanol solution (50%, 70%, 90%, and 100%, for 5 minutes each). After cleaning in alcohol-xylene mixtures (1:1 and then 1:6) and pure xylene, the slices were coverslipped with DPX mounting medium (Sigma-Aldrich).

GFAP Immunohistochemistry

The sections were permeabilized with 0.3% Triton X-100, blocked with 10% goat serum, and incubated in a rabbit monoclonal anti-GFAP antibody (1:200, Sigma-Aldrich) with 10% goat serum at 4°C overnight. Sections were then incubated in the goat anti-rabbit FITC IgG (Jackson Immunoresearch, West Grove, PA) secondary antibody for 1 hour at room temperature. Sections were coverslipped with Fluoromount-G (Southern Biotech, Birmingham, AL).

Quantification of Degenerative Changes

Neuronal and axonal degenerative changes were examined in the brains including the primary motor cortex, corpus callosum, and anterior commissure using an Olympus BX 60 microscope. Incidence of neuronal and axonal degeneration in these regions was recorded by 2 investigators blinded to the animal groups. A scale of 1 to 5 indices was used to indicate the number of animals demonstrating neuronal and axonal degeneration in a specific region after being subjected to different intensities of bTBI. An incidence of 1 indicates that degenerated neurons or axons were found in at least 1 of 5

randomly selected 20x magnification fields in the area. An incidence of 0 in a specific region means that no degenerative changes were found in that region (41). Axons with positive silver staining were traced using a Neurolucida system (MicroBrightField, Inc., Colchester, VT). The numbers of degenerative neurons in the motor cortex and positive axons in the corpus callosum were counted as described by Turner et al (61). Briefly, 2 slides from 1 sample were selected and a region of interest encompassing the motor cortex and corpus callosum was observed at low power using an Olympus BX-60 microscope and a Neurolucida system (MicroBrightField, Inc.). The number of cells and axons, respectively, was counted in a randomly selected field at 20x magnification (Olympus BX60). Changes in GFAP immunoreactivity in the motor cortex was also evaluated by counting the density of GFAP-positive cells using software Image J in a 20x magnification field. The ratio of the intensity value in the injury group to the sham group was calculated and analyzed.

Statistical Analysis

Statistical analysis was performed using SPSS 21.0 for Windows. The data are presented as mean ± SD. All data were analyzed by one-way or repeated-measures analyses of variance (ANOVA) as appropriate followed by individual Student-Neuman-Keuls test. Tukey's post hoc test was used for comparisons between and within groups and time points. A p value of < 0.05 was considered significant.

RESULTS

We developed a compact bTBI device that can be easily placed on a table (Fig. 1). Following more than 1000 blasts at various intensities, debris ejection never occurred. Nonetheless, we placed the open end of the shock tube directly toward a wall during the blasts. Noise-induced hearing loss is determined by either the intensity (dB) or duration of the exposure (62). The noise intensity measured 100 cm from the source was 90 dB and was uncomfortable.

Blast Explosion Under Different Pressure Intensities Induced Graded Shockwave Patterns

Shockwaves can be recorded in the driven chamber, measured by force sensors. A standard shockwave includes a sharp rise in the pressure wave followed by an immediate negative wave, as was induced by our bTBI device (Fig. 3A). The shockwave pattern replicated the response pattern from explosion as described by Friedlander (63). Additionally, shockwave intensities in our model can be predetermined to produce different bTBI severities. For example, pressures of 100, 200, and 250 psi induced graded shockwave intensities (Fig. 3A). The peak positive pressure in the driven chamber increased as the blast intensity increased from 100 to 250 psi. The reflective shockwave recordings, measured near the animal's head were 12 ± 2.6 at 100 psi, 50 ± 20.3 at 200 psi, and 100 ± 33.1 at 250 psi (Fig. 3B). Each incremental increase in pressure significantly raised the shockwave intensity ($p < 0.05$). The amplitude of the Friedlander shockwave induced by a 200 psi pressure was significantly higher than that induced by a 100 psi ($p < 0.05$). Likewise, the amplitude of the Friedlander shockwave induced by a 250 psi pressure was significantly higher than that induced by both a 100 and 200 psi blast ($p < 0.01$). Shockwaves generated by this device were 3 to 4 milliseconds long, and the positive phase of the shockwave lasted for approximately $\leq$0.5 milliseconds.

We determined that mice subjected to the 250 psi injury had a high mortality rate. In fact, 83% (19 of 23) mice died immediately after the 250 psi blast injury (Fig. 4). Although mice subjected to 100 and 200 psi blast injuries all survived (Fig. 4C), they demonstrated several behavioral and histological changes. Remarkably, when mice subjected to a 250 psi were protected by a body shield (Fig. 1D), the mortality rate decreased to 27% (7 of 26; Fig. 4C). Lung damage after 250 psi blast injury is demonstrated in Figure 4A. High-pressure shockwaves to unprotected lungs may cause alveolar over-expansion and collapse, which could be highly destructive. A body shield placed around the thorax and nose cone protected the chest/lungs from direct damage by the shockwave, thereby decreasing mortality.

Blast Injury Affects Vascular Permeability and Water Content of the Brain

Shockwaves that affect brain vasculature may be partially caused by an acute increase in the thoracic pressure resulting in rapid cerebral venous congestion. Figure 4B shows a brain exposed to a 250 psi blast injury as compared to a control brain from a mouse that received no blast injury. The injured brain demonstrated an increase in BBB permeability evidenced by erythrocyte extravasation (Fig. 4B). Alterations in the water content were analyzed by Evans Blue extravasation and brain water content. The percentages of water content of the whole brain were similar in all groups (sham group: 77.0%; 100 psi: 77.8%; 200 psi: 77.2%; and 250 psi: 78.5%), and there were no significant differences among the groups. However, Evans Blue extravasation showed increased vascular permeability that was observed only in the 250 psi blast injury group, which was significantly higher than in the sham, 100 psi, and 200 psi groups (Fig. 4D, $p < 0.05$).

Behavioral Effects of bTBI

Rotarod performance improved with pre-injury training of mice. The bTBI mice displayed minimal abnormalities of Rotarod performance between 1 and 7 days post-injury. No significant difference was found in Rotarod performance between the sham and all injury severity groups or between different injury severity groups ($p > 0.05$) (Fig. 5A).

Water maze performance was also improved following pre-injury training; this was manifested by shorter escape latencies in which the mouse could locate the submerged platform within 5 days (Fig. 5B) and stayed in the platform-quadrant longer after removal of the platform on the sixth day (Fig. 5C). The escape latency was significantly increased in mice subjected to a 250 psi bTBI. At days 4 to 5, the latency in the 250 psi group was significantly prolonged compared to all other groups including the sham group ($p < 0.05$). There were no differences between mice subjected to the 100 or

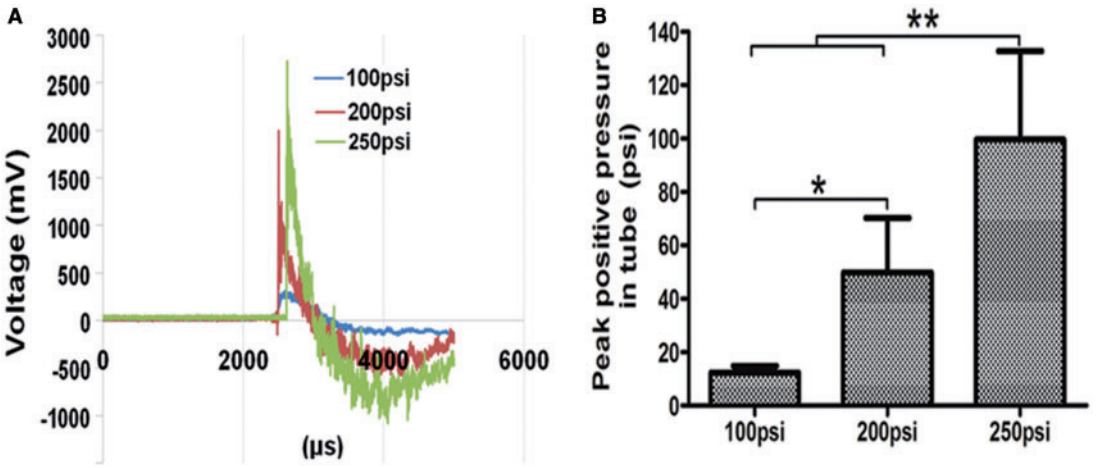

FIGURE 3. Generation of graded Friedlander waveforms. **(A)** A standard Friedlander waveform after a blast contains a positive peak followed by a negative phase. Shockwaves recorded in the driven chamber showed pressure-dependent amplitudes in response to 100, 200, and 250 psi blast. **(B)** Different pressures in the driver chamber resulted in corresponding levels of peak positive pressures measured in the driven chamber. Significant differences were found in peak positive pressures between the different driver chamber pressures (*$p < 0.05$, 200 psi vs. 100 psi; **$p < 0.01$, 250 psi vs. 100 and 200 psi).

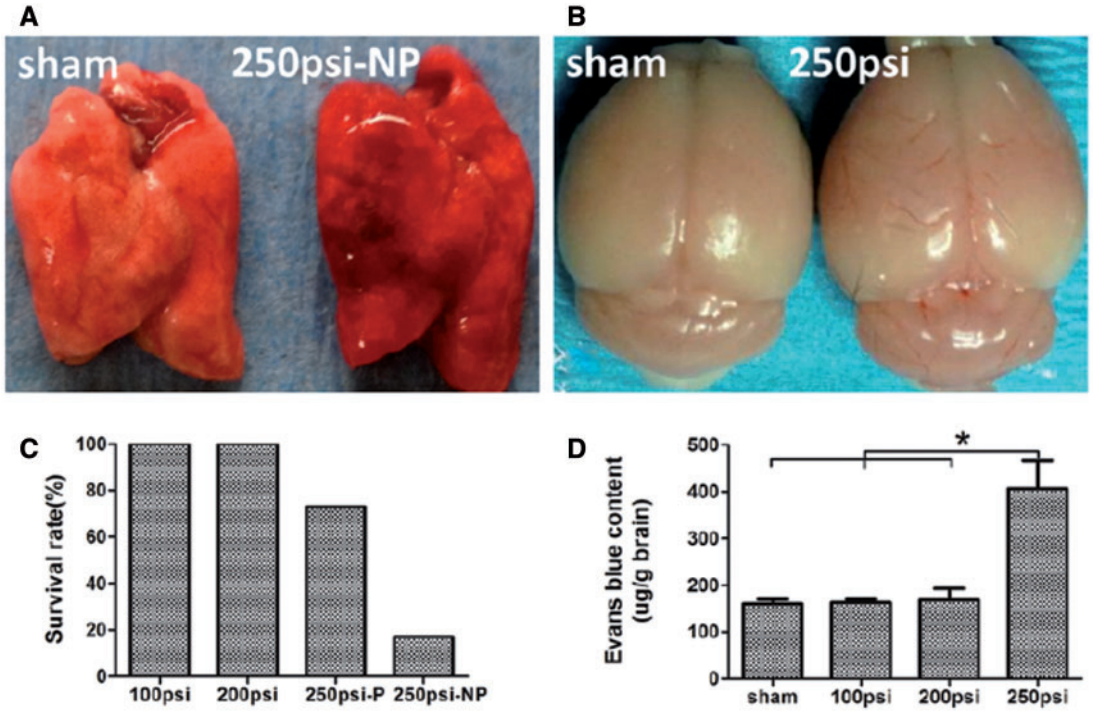

FIGURE 4. Effect of blast injury on lung damage, brain edema, and mortality. **(A)** Mice exposed to a 250 psi blast experienced apnea. Hemorrhagic changes were clearly seen in a mouse subjected to a 250 psi blast without a shield protection (right) as compared to the normal appearance of a sham control (left). **(B)** Gross appearance of a brain subjected to a 250 psi blast at 24 hours (right) compared to the sham (left). The blast-injured brain demonstrates severe edema and blood extravasation. **(C)** Survival rate of mice subjected to 100, 200, and 250 psi with and without body protection. It should be noted that 83% mice died in the 250 psi group with no shield protection (250 psi-NP). The survival was significantly improved when the body shield protection and nose cone were applied (250 psi-P). **(D)** Damage of blood-brain-barrier (BBB) permeability, assessed by an increased uptake of Evans blue, was only found in the group that received the 250 psi blast injury, as compared to the sham and 100 and 200 psi blast injury groups (*$p < 0.05$).

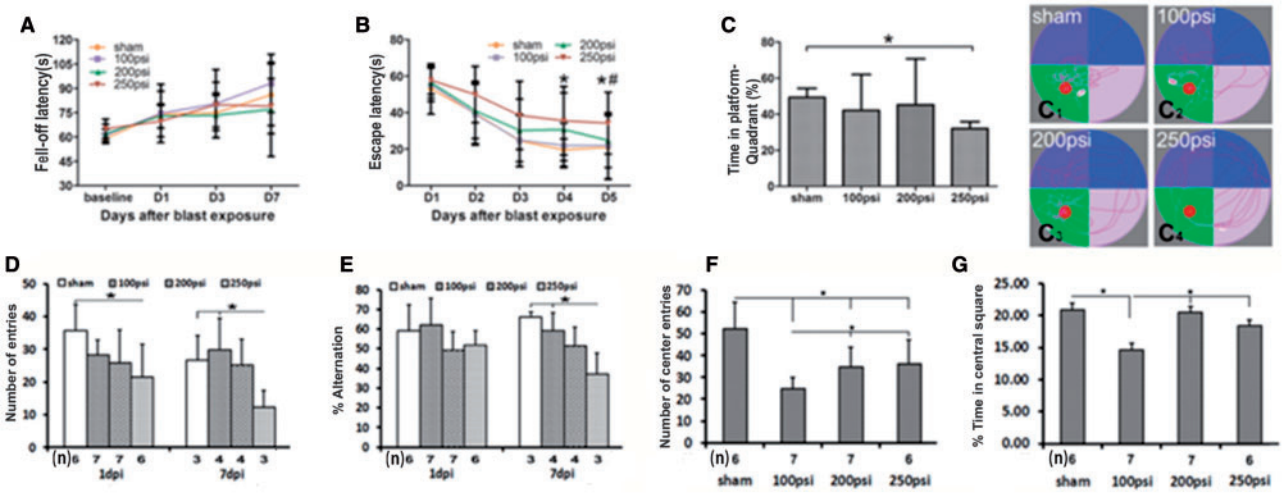

FIGURE 5. Behavioral changes after blast-induced traumatic brain injury (bTBI). **(A)** Rotarod test showed no significant locomotor differences among all treatment groups. **(B)** Morris water maze test showed a significant increase in the escape latency in the 250 psi injury group during the 5 day test period after bTBI (*$p < 0.05$ vs. sham; #$p < 0.05$ vs. 100 or 200 psi). **(C, C1-4)** Morris water maze test showed a significant decrease of time in platform-quadrant in the 250 psi group after the platform was removed (*$p < 0.05$ vs. sham). **(D)** Y maze test showed a significant decrease in the total number of arm entries of mice subjected to the 250 psi injuries on 1 and 7 days post injury (dpi) ($p < 0.05$ vs. sham). **(E)** The percentage of alternation in the 250 psi group was significantly decreased only on the 7th dpi ($p < 0.01$ vs. sham). **(F)** Open field exploration test showed a significant decrease in the number of central entry in all bTBI injury groups (*$p < 0.05$ vs. sham). There was also a significant decrease in the number of central entries between the 100 psi and the 200 and 250 psi groups (*$p < 0.05$). **(G)** Only the mildly injured mice (100 psi) showed a significant decrease in the percentage of time spent in the central square (*$p < 0.05$ vs. sham, 200 psi or 250 psi). Error bars: standard deviation. (n) = number of animals in **(D-G)**.

200 psi injury and the sham group ($p > 0.05$) (Fig. 5B). On the sixth day, the memory function was evaluated by recording the duration that animals lingered in the platform-quadrant after the platform was removed. The 250 psi injury group stayed the least time in the platform-quadrant compared to the sham group during the whole time of 60 seconds ($p < 0.05$) (Fig. 5C). There was no significant difference in speed among the tested groups (sham: 32.54 ± 5.42, 100 psi: 33.16 ± 6.74, 200 psi: 32.38 ± 5.97, and 250 psi: 31.95 ± 5.36; $p > 0.05$). The increased escape latency in mice subjected to a 250 psi bTBI indicates a poorer function of memory and learning in seeking the platform as compared with other groups. Because no difference in speed was found among all groups, the shock-wave injury likely had limited influence on locomotor function, which was also supported by the results of the Rotarod test (Fig. 5A, B).

The Y-maze performance was severely impaired in mice subjected to a 250 psi injury. There was a significant decrease in the number of times that mice entered the arms of the Y-maze at 1 and 7 days post-injury ($p < 0.05$) (Fig. 5D). The percentage of alternation also decreased on day 7 post-injury ($p < 0.05$) (Fig. 5E). Y-maze scores of mice exposed to 100 and 200 psi blast injuries were not significantly different from the sham control either in total entry or percentage of arm alternation ($p > 0.05$).

In the open field test, mice subjected to all levels of blast injuries demonstrated decreased entry into the region compared to the sham animals at 1 day post-injury ($p < 0.05$) (Fig. 5F). Mice subjected to a 100 psi blast injury demonstrated a shorter duration within the central square than those which received a 200 or 250 psi injury ($p < 0.05$) (Fig. 5G). One week later, no significant difference existed between all injury groups and sham group ($p < 0.05$, data not shown).

Blast Injury Induced Neuronal and Axonal Degeneration

Silver staining showed that increased blast injuries induced severity-dependent neuronal and axonal degeneration (Fig. 6A-N). In 2 selected regions of the brain, ie, the primary motor cortex and the external capsule, silver stained degenerated neurons and axons were found and their numbers increased when the injury severities increased (Fig. 6M-N, $p < 0.01$). Widespread neuronal and axonal damage was also observed in many other regions of the brain following a blast injury. The Table summarizes silver stained degeneration in different regions of the gray and white matters through 2 coronal sections of the brain: anterior commissure and mid-hippocampus. In these regions, neural and axonal degeneration was widely distributed including the anterior commissure, hippocampus, cortical gray matter, deep thalamic and basal ganglion nuclei, internal capsule, anterior commissure, external capsule, and the optic tract. Hippocampal degenerative changes were found in 2 of 5 mice that were subjected to the 250 psi blast. The extent of neuronal and axonal degeneration was slightly higher in the animals exposed to higher intensity injuries. Pathological characteristics of neuronal degeneration (Fig. 7A-N) were confirmed by FJB staining (Fig. 8A-D).

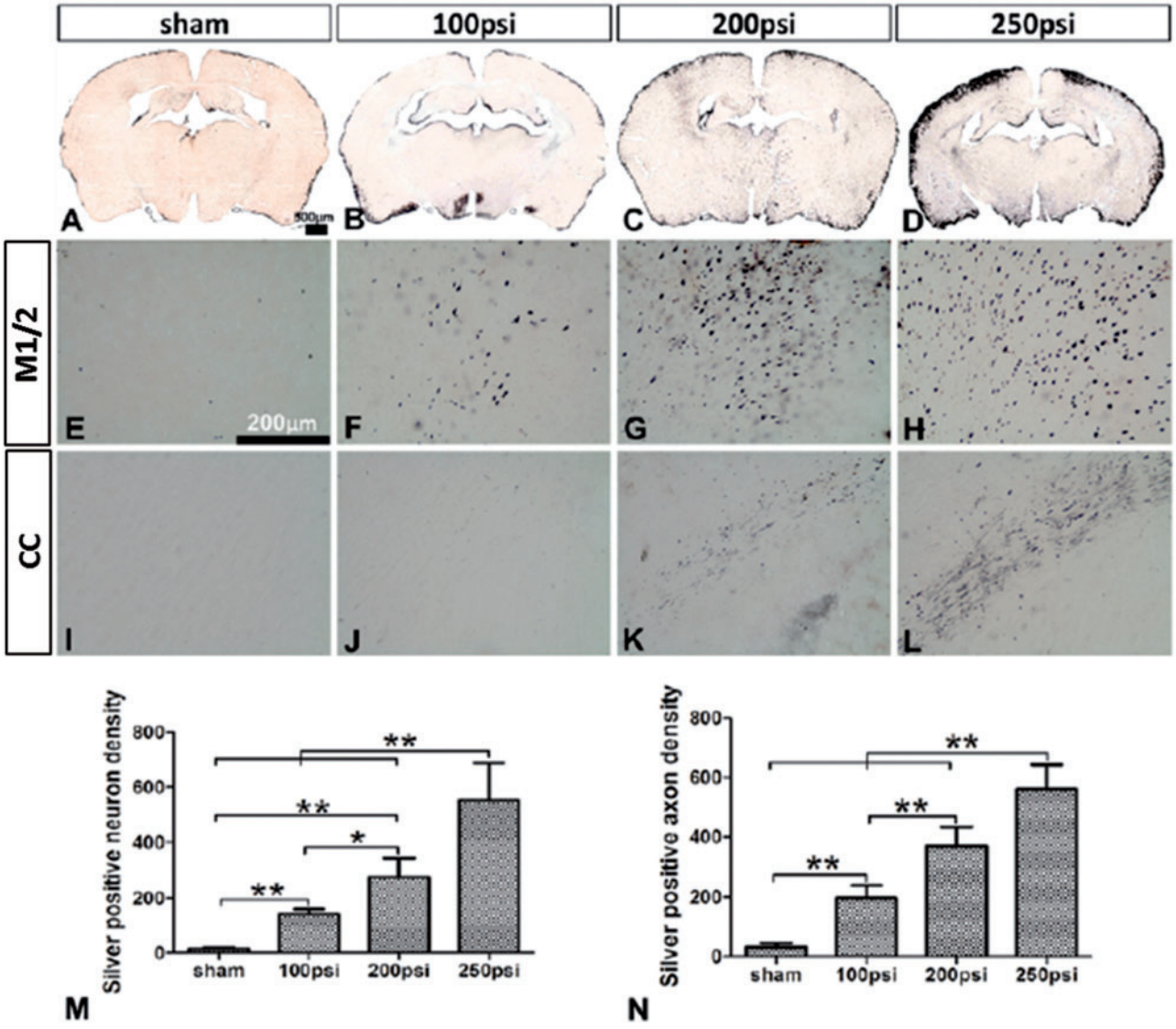

FIGURE 6. Neuronal and axonal degenerative changes in the brain following blast-induced traumatic brain injury (b-TBI). **(A-D)** Representative coronal sections of the brains showing silver staining in the sham and 3 graded bTBI groups. **(E-H)** In the motor cortex, there was dose-depending severity of neuronal degeneration in animals with blast injuries. **(I-L)** Axonal degeneration was found in the corpus callosum (CC) of injury groups compared to the sham. **(M, N)** Quantification of degenerating neurons (*$p < 0.05$; **$p < 0.01$, **M**) and axons (*$p < 0.01$, **N**) in the different groups.

Blast Injury-Induced Reactive Astrocytosis

Following bTBI the density of GFAP-positive astrocytes was increased and was injury severity-dependent (Fig. 8E-H). Reactive astrocytes increased significantly within the motor cortex in all blast injury groups as compared to the sham group (250 psi vs. sham: $p < 0.001$; 200 psi vs. sham $p < 0.01$; 100 psi vs. sham: $p < 0.05$). The degree of astrogliosis in response to bTBI was graded and severity-dependent (250 psi vs. 100 psi, $p < 0.01$; 250 psi vs. 200 psi, $p < 0.05$).

DISCUSSION

The bTBI studies would be optimal if performed in an open field that imitates true conditions in the battlefield (9); however, such an environment is not available for most research institutes. Studies of the effect of shockwaves in a confined space are the only choice despite the inherent shortcomings or limitations such as reflective load related to the areal occupancy of the mouse that does not reflect free field conditions. In this study, we report a novel compact blast-wave injury device that produces injuries by pre-determined membrane rupture with predetermined pressures

A Unique Mechanism of Producing Membrane Rupture With a Predetermined Pressure

Devices that produce experimental bTBI use compressed air in which the shockwave occurs at the point the

TABLE. Incidence of Neuronal and Axonal Degeneration in the Brain Based on Silver Staining

Group (n = 5)	Level I: Section Through the Anterior Commissure									
	Grey Matter						White Matter			
	M1/M2	S1HL/FL	S1BF	S2	Pir	MS	CC	CG	EC	AC
100 psi	4	3	4	3	1	1	3	3	2	3
200 psi	5	5	4	4	4	2	5	5	4	3
250 psi	5	5	5	4	5	3	5	5	4	3

Group (n = 5)	Level II: Section Through the Hippocampus										
	Grey Matter					White Matter					
	M1/M2	S1Tr	S1BF	S2	Pir	CC	CG	EC	IC	Opt	Hippocampus (CA2)
100 psi	3	4	3	3	3	4	4	4	3	1	0
200 psi	5	5	4	4	4	4	4	4	4	3	0
250 psi	5	5	5	5	4	5	5	4	5	4	2

AC, anterior commissure; CC, corpus callosum; CG, cingulum; EC, external capsule; IC, internal capsule; M1/M2, primary motor cortex/secondary motor cortex; MS, medial septal nucleus; Opt: optic tract; Pir, piriform cortex; S1BF, somatosensory 1, barrel field; S1HL/FL, somatosensory 1, forelimb region/hindlimb region; S1Tr, somatosensory 1, trunk region; S2, secondary somatosensory cortex. 1 to 5 indicates the numbers of animals demonstrating neuronal and axonal degeneration in each group after being subjected to different intensities of blast-induced traumatic brain injury (bTBI).

membrane ruptures. The polymer membrane is subjected to a high pressure within the driver chamber to the point of failure (Fig. 1A). Once the membrane ruptures, air from the driver chamber explodes into the driven chamber, generating a shockwave. In almost all other reported bTBI devices, the shockwave intensity that creates bTBI is dependent on the consistency of the quality and thickness of the membrane (17, 40, 41). The rupture points of the membranes having the same gauge or from the same roll may, however, differ. To reduce variability in pressures at which the membrane ruptures, we developed a unique mechanism of membrane perforation. In our case, controlled membrane rupture with a predetermined pressure in the driver chamber caused a predictable, controlled shockwave in the driven chamber. The shockwave in the driven chamber lasted 4 milliseconds. Shockwaves elicited by this mechanism should be more reliable than by spontaneous membrane rupture. Using our predetermined membrane rupture mechanism, 3 magnitudes of blast injuries were produced at 100, 200, and 250 psi. This model allows the generation of any injury severity by controlling the predetermined blast pressure within the driver chamber. Thus, this model can create different magnitudes of blast injuries, which is useful to study cellular and molecular mechanisms of bTBI.

Controlled Membrane Rupture With a Predetermined Pressure Allows the Generation of Graded Friedlander Curves

The simplest form of a blast wave has been described and termed the Friedlander waveform (40, 64). The magnitude of the Friedlander waveform in the driven chamber is measured by a pressure sensor, which can be influenced by its distance from the membrane and by its angle in the tubing that is subject to various reflective waves. Because mice in our study were all positioned facing the membrane at a fixed distance, the sensor was placed at the same location. Friedlander tracings showed incremental increases in amplitude as the blast pressure increased from 100 to 250 psi, indicating that we were able to generate graded pressurized shocks.

Head Stabilization and Thorax Protection of Mice Reduce Unanticipated Injuries and Death

Uncontrollable head movements such as acceleration-deceleration injuries during bTBI may increase the injury severity and variability. Such uncontrollable head movements could be reduced by wrapping the mice in a mesh net (65, 66). In our study, head movement was eliminated using a skull fixation device (Fig. 1C), which isolated the injury to solely the blast effect. Restriction of head motion prevents acceleration-deceleration injuries, therefore, reduces the risk of increasing the injury severity. Additionally, our head fixation device allows a rapid, effective, and simple placement of the mouse into the driven chamber during blast injury experiments.

We also found that a metal shield surrounding the thorax and nose cone can greatly decrease the magnitude of pulmonary and brain injuries and, therefore, decrease the mortality of mice receiving severe bTBI. Similar results were reported clinically using a Kevlar vest (6, 67). Protection of the lungs from barotrauma is of value in mitigating cerebral injury following bTBI. Without lung protection, animals survived when the bTBI was $\leq$200 psi. However, when the pressure reached 250 psi, there was a high incidence of respiratory failure and death, similar to what was reported by Long et al (6). A pressure of 250 psi caused extensive BBB permeability. These results suggest that protection from pulmonary barotrauma using

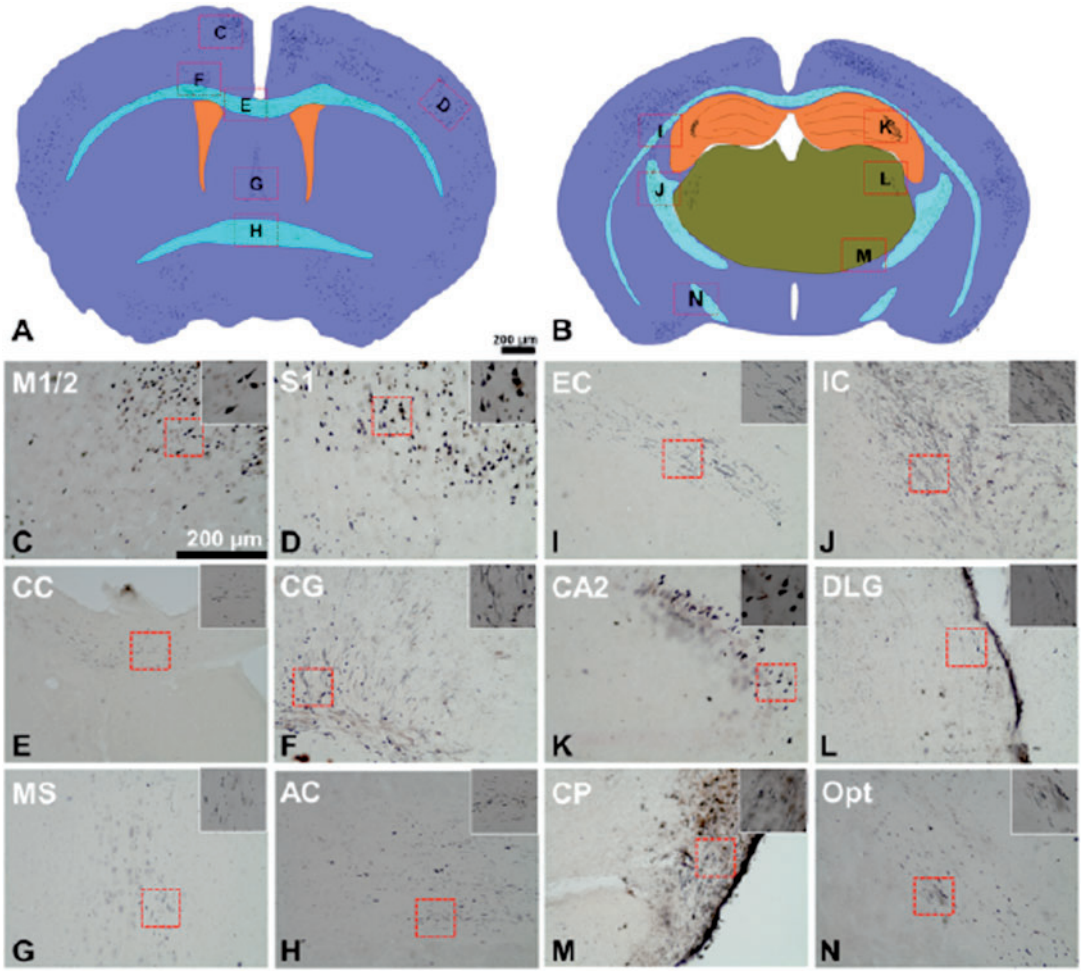

FIGURE 7. Silver staining demonstrates neuronal and axonal degeneration. **(A, B)** Representative plots of degenerative changes shown at 2 coronal sectional levels that cut through the anterior commissure **(A)** and hippocampus **(B)** following a 250 psi blast exposure. **(C-H)** At the anterior commissure level, silver staining showed degenerative changes in primary and secondary motor cortex (M1/2, **C**); primary sensory cortex (S1, **D**), corpus callosum (CC, **E**), cingulum (CG, **F**), medial septal nucleus (MS, **G**), and anterior commissure AC, **(H)**. **(I-N)** At the hippocampus level, silver staining showed degenerative changes in external capsule (EC, **I**); internal capsule (IC, **J**), CA 2 region of the hippocampus (CA2, **K**), dorsolateral geniculate nucleus (DLG, **L**), cerebral peduncle (CP, **M**), and optic tract (Opt, **N**). Inserts in upper right corners of C-N show high magnification images of boxed areas of corresponding images. Letters in **(A)** and **(B)** correspond to panels **(C-N)**. Scale bars: 200 µm.

a thoracic protective shield and nose cone may ameliorate brain damage and improve survival.

The Shockwave Duration Is Determined by the Volume of Gas Within the Driven Chamber

In our model, shockwaves elicited in the driven chamber lasted 4 milliseconds. As the pressure increased from 200 to 250 psi, the amplitude of the shockwave doubled (Fig. 3B). The brief shockwave duration is a result of the small volume of gas within the driver chamber. The magnitude of the blast injury is a function of both the pressure and volume of compressed gas within the driver chamber. Because of the small volume of gas within the driver chamber, a greater pressure is required to produce the injury (40). The present study clearly indicates the importance of the shockwave duration in creating bTBI. Using short duration and low amplitude shockwaves, no lung injury was observed, with only minimal cortical and hippocampal injury. Our observations are similar to those of Park et al for bTBI caused by shockwaves $\leq$200 psi (68). Shockwaves induced by 250 psi pressure having a short duration caused fatal lung barotrauma and distinct brain damage. This phenomenon suggests that injury magnitude is based on the amplitude as well as shockwave duration (69). The duration of the entire shockwave that we measured was short due to the small volume of air in the driver chamber, which was a drawback of the model. Other models with larger driver chambers and longer driven tubes produce longer shockwaves. For example, Reneer et al used a blast device that was 19 feet long, and they recorded shockwaves for 20

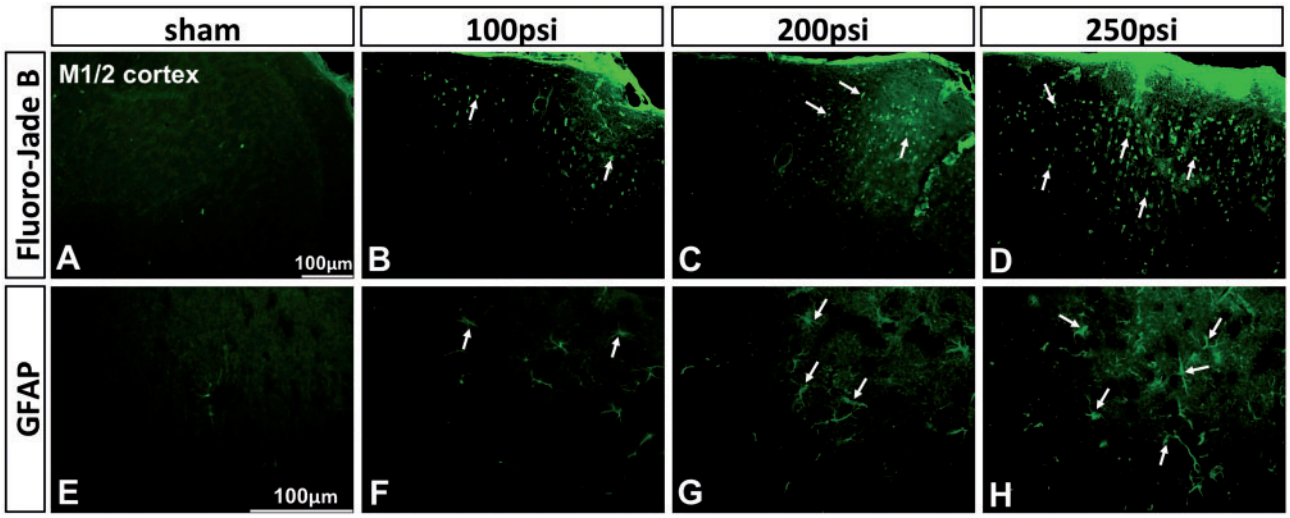

FIGURE 8. Neuronal degeneration and glial responses after blast-induced traumatic brain injury (bTBI). **(A)** Fluoro-Jade B (FJB) staining showed the lack of staining in the sham control of the M1/2 motor cortex. **(B-D)** bTBI produced severity-related increase in FJB-stained neurons at 7 days post-injury. **(E-H)** bTBI induced severity-related astrocytic responses in the M1/2 region at 7 days post-injury. Reactive astrocytes show enhanced GFAP immunoreactivity, elongated processes, and enlarged cell bodies (arrows). Scale bars: 100 μm.

milliseconds. In that study the magnitude of the negative pressure wave was minimal and reached a peak at < 8 milliseconds, producing a significant brain injury (14). Clearly, both duration and amplitude of the shockwave are key parameters in creating and predicting the severity of bTBI. Transmission of shockwaves through the brain and factors influencing the energy decay are still unknown (17). Understanding these issues would facilitate the development of strategies for the prevention and amelioration of the effects of bTBIs.

bTBI Induced Cognitive and Emotional Changes

In the present study, cognitive abnormalities as assessed by the Morris water maze were observed as pressures increased from 100 psi to 250 psi. Cognitive functions deteriorated as the intensity of blast injuries increased from moderate to severe (200–250 psi) with clearly identified neuronal degenerative changes. Consistently, Y maze testing also showed that mice with 250 psi injury lost their exploratory capability and did not recover within 1 week. Further, the spatial working memory significantly declined 1 week after the injury. The changes of cognitive function were similar to those of previous blast brain injury studies, which were related to the shockwave intensity (40, 70, 71). However, our study only showed that the motor dysfunction trended downward but did not reach the statistically significant level as shown in another study with an uncontrollable blast device (40).

bTBI produced in this model is a valuable experimental tool because it closely replicates clinical injuries seen in combat trauma, in particular, cumulative effects of bTBI. Consistent with previous reports (71, 72), the open-field test demonstrated that a single blast (100 psi) temporarily resulted in a lower exploratory behavior and a greater level of anxiety than more severe injuries.

bTBI Induced Injury Severity-Related Histopathological Changes

Detailed neuropathological analyses are essential for understanding the mechanisms of bTBI (15, 65, 73). We demonstrate that bTBI caused injury severity-related histopathological changes. Neuronal degeneration was detected by both FJB staining at 24 hours and silver staining at 7 days post-injury. Silver staining also detected axonal degeneration in various regions of the white matter. Additionally, increased astrogliosis, indicated by increased GFAP immunoreactivity, was observed at 7 days post-injury. Our findings confirm previously published work by Turner et al using a rat model (61). Silver staining provided a very sensitive measurement of the extent and severity of neuronal and axonal degeneration at 7 days post bTBI. Neural degeneration was most prominent in the cerebral cortex (74). We observed widespread degeneration in multiple regions of the white and gray matter. These results indicate that neural and axonal degeneration, as well as astrocytic activation, may be realistic targets for neuroprotection and recovery of function. These degenerating neurons and axons and activated astrocytes may also be used as markers for measuring the severity of brain damage and repair after bTBI (Table).

In summary, a major advantage of our compact bTBI system is its small size, which can be placed easily on a table. Another advantage of the system is that the air pressure can be predetermined to rupture the membrane so that injuries of different severities may be chosen. Using such a compact bTBI device, controlled, predictable, and reproducible shockwaves to mice were produced that induced correlative cognitive and

pathological changes. This model could be particularly useful for those using genetically modified mice to study specific genes or molecules that influence neurological and cognitive dysfunction following bTBI or to screen for putative treatments.

REFERENCES

1. Armonda RA, Bell RS, Vo AH, et al. Wartime traumatic cerebral vasospasm: Recent review of combat casualties. Neurosurgery 2006; 59:1215–25
2. Chen Y, Huang W. Non-impact, blast-induced mild TBI and PTSD: Concepts and caveats. Brain Inj 2011;25:641–50
3. DePalma RG, Burris DG, Champion HR, et al. Blast injuries. N Engl J Med 2005;352:1335–42
4. Garner J, Brett SJ. Mechanisms of injury by explosive devices. Anesthesiol Clin 2007;25:147–60
5. Lew HL, Poole JH, Alvarez S, et al. Soldiers with occult traumatic brain injury. Am J Phys Med Rehabil 2005;84:393–8
6. Long JB, Bentley TL, Wessner KA, et al. Blast overpressure in rats: Recreating a battlefield injury in the laboratory. J Neurotrauma 2009; 26:827–40
7. Taber KH, Warden DL, Hurley RA. Blast-related traumatic brain injury: What is known? J Neuropsychiatry Clin Neurosci 2006;18:141–5
8. Warden D. Military TBI during the Iraq and Afghanistan wars. J Head Trauma Rehabil 2006;21:398–402
9. Needham CE, Ritzel D, Rule GT, et al. Blast testing issues and TBI: Experimental models that lead to wrong conclusions. Front Neurol 2015;6:72
10. Bauman RA, Ling G, Tong L, et al. An introductory characterization of a combat-casualty-care relevant swine model of closed head injury resulting from exposure to explosive blast. J Neurotrauma 2009;26:841–60
11. Cullen DK, Xu Y, Reneer DV, et al. Color changing photonic crystals detect blast exposure. Neuroimage 2011;54:S37–S44
12. Kuehn R, Simard PF, Driscoll I, et al. Rodent model of direct cranial blast injury. J Neurotrauma 2011;28:2155–69
13. Pun PB, Kan EM, Salim A, et al. Low level primary blast injury in rodent brain. Front Neurol 2011;2:19
14. Reneer DV, Hisel RD, Hoffman JM, et al. A multi-mode shock tube for investigation of blast-induced traumatic brain injury. J Neurotrauma 2011;28:95–104
15. Risling M, Plantman S, Angeria M, et al. Mechanisms of blast induced brain injuries, experimental studies in rats. Neuroimage 2011;54:S89–S97
16. Axelsson H, Yelverton JT. Chest wall velocity as a predictor of nonauditory blast injury in a complex wave environment. J Trauma 1996;40:S31–S37
17. Nakagawa A, Manley GT, Gean AD, et al. Mechanisms of primary blast-induced traumatic brain injury: Insights from shock-wave research. J Neurotrauma 2011;28:1101–19
18. Courtney MW, Courtney AC. Note: A table-top blast driven shock tube. Rev Sci Instrum 2010;81:126103
19. Ahmad A, Crupi R, Campolo M, et al. Absence of TLR4 reduces neurovascular unit and secondary inflammatory process after traumatic brain injury in mice. PLoS One 2013;8: e57208
20. Bachstetter AD, Rowe RK, Kaneko M, et al. The p38alpha MAPK regulates microglial responsiveness to diffuse traumatic brain injury. J Neurosci 2013;33: 6143–53
21. Kelso ML, Scheff SW, Pauly JR, et al. Effects of genetic deficiency of cyclooxygenase-1 or cyclooxygenase-2 on functional and histological outcomes following traumatic brain injury in mice. BMC Neurosci 2009;10:108
22. Ley EJ, Clond MA, Singer MB, et al. IL6 deficiency affects function after traumatic brain injury. J Surg Res 2011;170: 253–6
23. Ley EJ, Clond MA, Bukur M, et al. Beta-adrenergic receptor inhibition affects cerebral glucose metabolism, motor performance, and inflammatory response after traumatic brain injury. J Trauma Acute Care Surg 2012;73:33–40
24. Longhi L, Perego C, Ortolano F, et al. Tumor necrosis factor in traumatic brain injury: Effects of genetic deletion of p55 or p75 receptor. J Cereb Blood Flow Metab 2013;33:1182–9
25. Strauss KI, Gruzdev A, Zeldin DC. Altered behavioral phenotypes in soluble epoxide hydrolase knockout mice: Effects of traumatic brain injury. Prostaglandins Other Lipid Mediat 2013;104-105:18–24
26. Tanaka Y, Matsuwaki T, Yamanouchi K, et al. Exacerbated inflammatory responses related to activated microglia after traumatic brain injury in progranulin-deficient mice. Neuroscience 2013;231:49–60
27. Zhang YP, Cai J, Shields LBE, et al. Traumatic brain injury using mouse models. Transl Stroke Res 2014;5:454–71
28. Albert-Weissenberger C, Stetter C, Meuth SG, et al. Blocking of bradykinin receptor B1 protects from focal closed head injury in mice by reducing axonal damage and astroglia activation. J Cereb Blood Flow Metab 2012;32:1747–56
29. Cai W, Carlson SW, Brelsfoard JM, et al. Rit GTPase signaling promotes immature hippocampal neuronal survival. J Neurosci 2012;32:9887–97
30. Cheng ZG, Zhang GD, Shi PQ, et al. Expression and antioxidation of Nrf2/ARE pathway in traumatic brain injury. Asian Pac J Trop Med 2013;6:305–10
31. Hong Y, Yan W, Chen S, et al. The role of Nrf2 signaling in the regulation of antioxidants and detoxifying enzymes after traumatic brain injury in rats and mice. Acta Pharmacol Sin 2010;31:1421–30
32. Kabadi SV, Stoica BA, Loane DJ, et al. Cyclin D1 gene ablation confers neuroprotection in traumatic brain injury. J Neurotrauma 2012;29:813–27
33. Krajewska M, You Z, Rong J, et al. Neuronal deletion of caspase 8 protects against brain injury in mouse models of controlled cortical impact and kainic acid-induced excitotoxicity. PLoS One 2011;6: e24341
34. Walker KR, Kang EL, Whalen MJ, et al. Depletion of GGA1 and GGA3 mediates postinjury elevation of BACE1. J Neurosci 2012;32:10423–37
35. Corrigan F, Thornton E, Roisman LC, et al. The neuroprotective activity of the amyloid precursor protein against traumatic brain injury is mediated via the heparin binding site in residues 96-110. J Neurochem 2014;128:196–204
36. Doering P, Stoltenberg M, Penkowa M, et al. Chemical blocking of zinc ions in CNS increases neuronal damage following traumatic brain injury (TBI) in mice. PLoS One 2010;5:e10131
37. Mannix RC, Zhang J, Park J, et al. Detrimental effect of genetic inhibition of B-site APP-cleaving enzyme 1 on functional outcome after controlled cortical impact in young adult mice. J Neurotrauma 2011;28: 1855–61
38. Marklund N, Morales D, Clausen F, et al. Functional outcome is impaired following traumatic brain injury in aging Nogo-A/B-deficient mice. Neuroscience 2009;163:540–51
39. Theus MH, Ricard J, Bethea JR, et al. EphB3 limits the expansion of neural progenitor cells in the subventricular zone by regulating p53 during homeostasis and following traumatic brain injury. Stem Cells 2010; 28:1231–42
40. Cernak I, Merkle AC, Koliatsos VE, et al. The pathobiology of blast injuries and blast-induced neurotrauma as identified using a new experimental model of injury in mice. Neurobiol Dis 2011;41:538–51
41. Koliatsos VE, Cernak I, Xu L, et al. A mouse model of blast injury to brain: initial pathological, neuropathological, and behavioral characterization. J Neuropathol Exp Neurol 2011;70:399–416
42. Wang Y, Wei Y, Oguntayo S, et al. Tightly coupled repetitive blast-induced traumatic brain injury: Development and characterization in mice. J Neurotrauma 2011;28:2171–83
43. Alphonse VD, Siva Sai SS,V, Kemper, AR, et al. Membrane characteristics for biological blast overpressure testing using blast simulators. Biomed Sci Instrum 2014;50:248–53
44. Leonardi AD, Bir CA, Ritzel DV, et al. Intracranial pressure increases during exposure to a shockwave. J Neurotrauma 2011;28:85–94
45. Zhu F, Mao H, Dal Cengio LA, et al. Development of an FE model of the rat head subjected to air shock loading. Stapp Car Crash J 2010; 54:211–25
46. Liu NK, Zhang YP, O'Connor J, et al. A bilateral head injury that shows graded brain damage and behavioral deficits in adult mice. Brain Res 2013;1499:121–8
47. Morris R. Developments of a water-maze procedure for studying spatial learning in the rat. J Neurosci Methods 1984;11:47–60
48. Dellu F, Mayo W, Cherkaoui J, et al. A two-trial memory task with automated recording: Study in young and aged rats. Brain Res 1992; 588:132–9
49. Sarter M, Bodewitz G, Stephens DN. Attenuation of scopolamine-induced impairment of spontaneous alteration behaviour by antagonist but not inverse agonist and agonist beta-carbolines. Psychopharmacology (Berl) 1988;94:491–5

50. Podhorna J, Brown RE. Strain differences in activity and emotionality do not account for differences in learning and memory performance between C57BL/6 and DBA/2 mice. Genes Brain Behav 2002;1:96–110
51. Podhorna J, McCabe S, Brown RE. Male and female C57BL/6 mice respond differently to diazepam challenge in avoidance learning tasks. Pharmacol Biochem Behav 2002;72:13–21
52. Liu WY, Wang ZB, Wang Y, et al. Increasing the permeability of the blood-brain barrier in three different models in vivo. CNS Neurosci Ther 2015;21:568–74
53. Marchi N, Banjara M, Janigro D. Blood-brain barrier, bulk flow, and interstitial clearance in epilepsy. J Neurosci Methods 2015 [Epub ahead of print] doi: 10.1016/j.jneumeth.2015.06.011.
54. Rojiani AM, Prineas JW, Cho ES. Electrolyte-induced demyelination in rats. 1. Role of the blood-brain barrier and edema. Acta Neuropathol 1994;88:287–92
55. Watanabe O, West CR, Bremer A. Experimental regional cerebral ischemia in the middle cerebral artery territory in primates. Part 2: Effects on brain water and electrolytes in the early phase of MCA stroke. Stroke 1977;8:71–6
56. Schmued LC, Hopkins KJ. Fluoro-Jade B: A high affinity fluorescent marker for the localization of neuronal degeneration. Brain Res 2000;874:123–30
57. Schmued LC, Hopkins KJ. Fluoro-Jade: Novel fluorochromes for detecting toxicant-induced neuronal degeneration. Toxicol Pathol 2000;28:91–9
58. Schmued LC, Beltramino C, Slikker W, Jr. Intracranial injection of Fluoro-Gold results in the degeneration of local but not retrogradely labeled neurons. Brain Res 1993;626:71–7
59. de Olmos JS, Beltramino CA, de Olmos de LS. Use of an amino-cupric-silver technique for the detection of early and semiacute neuronal degeneration caused by neurotoxicants, hypoxia, and physical trauma. Neurotoxicol Teratol 1994;16:545–61
60. Hall ED, Bryant YD, Cho W, et al. Evolution of post-traumatic neurodegeneration after controlled cortical impact traumatic brain injury in mice and rats as assessed by the de Olmos silver and fluorojade staining methods. J Neurotrauma 2008;25:235–47
61. Turner RC, Naser ZJ, Logsdon AF, et al. Modeling clinically relevant blast parameters based on scaling principles produces functional & histological deficits in rats. Exp Neurol 2013;248:520–9
62. Bolm U, Brundel KH. [Extent and frequency of noise-induced hearing loss in miners depending on the intensity and duration of noise exposure]. HNO 1979;27:351–4
63. Friedlander FG. The diffraction of sound pulses; on a paradox in the theory of reflexion. Proc R Soc Lond A Math Phys Sci 1946;186:356–67
64. Sundaramurthy A, Alai A, Ganpule S, et al. Blast-induced biomechanical loading of the rat: An experimental and anatomically accurate computational blast injury model. J Neurotrauma 2012;29:2352–64
65. Magnuson J, Leonessa F, Ling GS. Neuropathology of explosive blast traumatic brain injury. Curr Neurol Neurosci Rep 2012;12:570–9
66. Risling M, Davidsson J. Experimental animal models for studies on the mechanisms of blast-induced neurotrauma. Front Neurol 2012;3:30
67. Cheng J, Gu J, Ma Y, et al. Development of a rat model for studying blast-induced traumatic brain injury. J Neurol Sci 2010;294:23–8
68. Park E, Gottlieb JJ, Cheung B, et al. A model of low-level primary blast brain trauma results in cytoskeletal proteolysis and chronic functional impairment in the absence of lung barotrauma. J Neurotrauma 2011; 28:343–57
69. Moochhala SM, Lu J, Xing MC, et al. Mercaptoethylguanidine inhibition of inducible nitric oxide synthase and cyclooxygenase-2 expressions induced in rats after fluid-percussion brain injury. J Trauma 2005; 59:450–7
70. Cernak I, Wang Z, Jiang J, et al. Cognitive deficits following blast injury-induced neurotrauma: Possible involvement of nitric oxide. Brain Inj 2001;15:593–612
71. Kovesdi E, Kamnaksh A, Wingo D, et al. Acute minocycline treatment mitigates the symptoms of mild blast-induced traumatic brain injury. Front Neurol 2012;3:111
72. Elder GA, Dorr NP, De GR, et al. Blast exposure induces post-traumatic stress disorder-related traits in a rat model of mild traumatic brain injury. J Neurotrauma 2012;29:2564–75
73. Garman RH, Jenkins LW, Switzer RC, III, et al. Blast exposure in rats with body shielding is characterized primarily by diffuse axonal injury. J Neurotrauma 2011;28:947–59
74. Gao X, Chen J. Mild traumatic brain injury results in extensive neuronal degeneration in the cerebral cortex. J Neuropathol Exp Neurol 2011;70: 183–91